Abstract

# Multiphase carbonate cementation related to fractures in the Upper Jurassic limestones, Maestrat Basin (Iberian Range, Spain)

Miguel Ángel Caja[a,1], Ihsan S. Al-Aasm[b,*], Rafaela Marfil[a,1], Meaza Tsige[c], Tomás Martín-Crespo[d,2], Ramón Salas[e]

[a] *Dpto. de Petrología y Geoquímica, Univ. Complutense de Madrid, 28040-Madrid, Spain*
[b] *Department of Earth Sciences, School of Physical Sciences, University of Windsor, 401 Sunset Avenue, Windsor, Ontario, Canada N9B 3P4*
[c] *Dpto. de Geodinámica, Univ. Complutense de Madrid, 28040-Madrid, Spain*
[d] *Dpto. de Cristalografía y Mineralogía, Univ. Complutense de Madrid, 28040-Madrid, Spain*
[e] *Departament de Geoquímica, Petrologia i Prospecció Geológica Facultat de Geología, Martí i Franquès, s/n Universitat de Barcelona, 08028 Barcelona, Spain*

**Abstract**

In the western part of the Penyagolosa subbasin (Maestrat Basin, Spain), carbonate cementation occludes fractures and infills stylolites in Tithonian–Berriasian limestones. Field relationships, petrography, cathodoluminesence and geochemical analyses (microprobe, fluid inclusions, oxygen, carbon and strontium isotopes) of the carbonate cements show that the paragenetic sequence includes (A) calcite cements in echelon tension gashes ($-11.37$‰ $\delta^{18}$O VPDB). (B) Scarce isolated rhombic dolomite replacement cement. (C) Saddle dolomite replacement cement with fluid inclusions that are characterized by high salinity (21.5 to 23.5% wt. eq. NaCl), high temperatures (Th 110–155 °C) and similar negative values of oxygen isotopes ($-11.27$‰ $\delta^{18}$O VPDB). (D) Calcite replacing (dedolomite) saddle and rhombic dolomite ($-8.61$ to $-6.76$‰ $\delta^{18}$O VPDB and $-4.38$ to $+0.07$‰ $\delta^{13}$C VPDB). (E) Calcite cement filling vertical fractures. They have the highest Th (160–260 °C), negative values of oxygen isotopes ($-9.97$ to $-13.44$‰ $\delta^{18}$O VPDB). (F) Calcite cement filling bed-parallel stylolites ($-8.81$‰ $\delta^{18}$O VPDB). This paragenetic sequence reflects multiple phases of fracture-controlled carbonate cements. The first stage calcite is related to syn-sedimentary rifting of the Late Jurassic–Early Cretaceous and progressive burial depth. The later phases of dolomite and calcite in vertical veins are considered hydrothermal in origin and indicate a mix of saline waters, possibly derived from the underlying Triassic and Liassic evaporites, with deep circulating meteoric water with higher temperature than the surrounding rocks and related to the regional Alpine compression.

*Keywords:* Carbonate cement; Geochemistry; Fractures; Maestrat Basin; Spain

## 1. Introduction

The Maestrat Basin (Fig. 1) is located in the eastern part of the Iberian rift system, and the Penyagolosa sub-basin is one of seven sub-basins formed during the Mesozoic rift stage (Salas et al., 2001). This paper addresses the field relationships, petrography and geochemistry of the carbonate cements that occlude fractures and infill stylolites. The paragenetic sequence, the geochemical signature of fluids and their relationship to the tectonic evolution of the basin are the focus of this study. Veins and stylolites occur in oncolitic limestones of the Tithonian–early Berriasian (Bovalar Formation). These limestones are massive or stratified with a total thickness of approximately 100 m. The formation is bounded by two unconformities. The sedimentation is related to the latest Oxfordian–late Hauterivian subsidence phase suggested for the Maestrat Basin. It comprised an initial period of fault-controlled, rapid, syn-rift subsidence, followed by a post-rift interval of decreasing subsidence, controlled by thermal relaxation of the lithosphere (Salas et al., 2001).

## 2. Sampling and analytical methods

The study section is located close to the Cedrillas trending normal fault. It was selected for this study because of the quality and abundance of cemented veins and stylolites. Strikes and dips were measured on a wide range of veins and bed-parallel stylolites in the Bovalar Formation. Forty-one samples were collected and double-polished thin sections were prepared from each sample and stained for carbonates (alizarine red-s and potassium ferricyanide). Thin sections were examined by conventional and cathodoluminescence (CL) petrography. CL petrography was carried out with a Technosyn cold cathodoluminescence model 8200 MK4.

The chemical composition of carbonate cements was determined by wavelength-dispersive X-ray spectrometry using a JEOL JXA-8900 electron microprobe (15 kV accelerating voltage, 21.5 nA beam current, 5 μm beam size). Detection limits were approximately 100 ppm for Mg, 150 ppm for Ca, 250 ppm for Mn and 300 ppm for Fe. The results were normalized to 100 mol% $CaCO_3$, $MgCO_3$, $FeCO_3$ and $MnCO_3$.

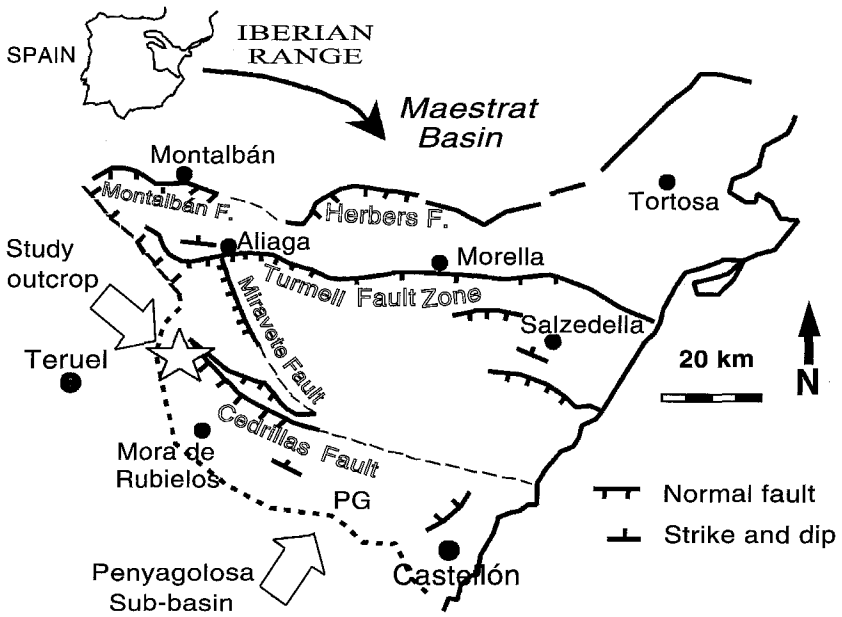


Fig. 1. Location map of the study area showing the main structural elements of Maestrat Basin (Salas et al., 2001).

Micro-thermometric characterization of fluid inclusion (FI) was performed using a Linkam THMSG 600 stage. The stage was calibrated with the melting point of solid standards at $T>25$ °C and natural and synthetic inclusions at $T<0$ °C.

Oxygen and carbon isotopes were measured on 21 samples of calcite and dolomite that were collected using a microscope-mounted microdrill assembly. The samples were reacted in vacuo with 100% pure phosphoric acid for over 4 h at 25 and 50 °C, respectively (Al-Aasm et al., 1990). The evolved $CO_2$ gas was analysed for isotopic ratios on a Delta-Plus mass spectrometer. Values of O and C isotopes are reported in per mill relative to VPDB standard. Precision was better than 0.05‰ for both isotopes. Strontium isotopes were analysed on 13 powdered calcite samples using a VG Sector 54 multi-collector mass spectrometer TIMS. The standard used was NBS-987 and the $2\sigma$ for a single measurement was better than 0.00003.

## 3. Results

Field and petrographic and CL investigations of the studied carbonates resulted in the identification of several textural and compositional types of carbonate cements. The paragenetic sequence includes five calcite phases and two dolomite phases (Table 1).

### *3.1. Echelon tension gashes calcite cement*

The first phase of calcite fills the echelon veins that form a net of tension gashes cross-cut by bed-parallel stylolites. This cement shows a prismatic texture with stretched fibres (100 to 390 μm), which are perpendicular to the vein wall. The chemical composition is ($Ca_{0.983}$ $Mg_{0.010}$ $Fe_{0.007}$ $Mn_0$) $CO_3$ ($n=12$). This calcite has negative values of $\delta^{18}O$ (−11.37‰ VPDB), but there is no significant difference in $\delta^{13}C$ (+1.06‰) with respect to the host rock and the other phases of cements, except for the dedolomite phase (see Fig. 2).

### *3.2. Veins*

Samples were obtained from several extensional veins, predominantly two sets with sub-vertical orientation (3.2.1.) and another set with bed-parallel orientation (3.2.2.).

#### *3.2.1. Vertical veins filled by calcite and dolomite replacement cements*

The following dolomite and calcite phases fill vertical extensional veins associated to the first stage ENE trend Alpine compression (Alvaro et al., 1979; Liesa and Simón, 1994). They are the most dominant fractures in this area and where four types of replacement cement are recognized.

*3.2.1.1. Rhombic dolomite.* Rhombic dolomite consists of scattered rhombs (up to 800 μm), showing on CL as a black nonluminescent core with a thin outer zone of bright orange that alternates with bright yellow calcite. The chemical composition of the rhombic dolomite is ($Ca_{0.548}$ $Mg_{0.415}$ $Fe_{0.036}$ $Mn_0$) $CO_3$ ($n=11$). This phase has a higher content of $FeCO_3$ (3.61 mol%) than the saddle dolomite. Isotopic analyses were not performed due to the phases' isolated occurrence.

*3.2.1.2. Saddle dolomite.* Saddle dolomite occurs as a thin dolomitized rim lining the margins of fractures. It also occurs in an "intense dolomitization zone" of the host rock (oncolitic limestone) that is probably related to a vertical fracture plane (like a "pipe-shaped structure"). Saddle dolomite shows curved faced crystals, sweeping extinction and under CL displays dull brown to nonluminescent colours. The chemical composition is ($Ca_{0.537}$ $Mg_{0.448}$ $Fe_{0.015}$ $Mn_0$) $CO_3$ ($n=48$). The $FeCO_3$ content is low (1.54 mol%). Homogenization temperatures (Th) and salinity were measured in primary fluid inclusions. Th values vary from 110 to 155 °C (mode = 125 °C) and the salinity range is from 21.5 to 23.5 wt.% NaCl eq. (mode = 22.5). Eutectic temperatures lower than −40 °C are characteristic of the $H_2O$–NaCl–($CaCl_2$) system. The $\delta^{18}O$ values range from −11.54 to −11.28, and $\delta^{13}C$ has positive values from +2.13 to +2.22 (Fig. 2).

*3.2.1.3. Dedolomite.* In these calcite crystals, the typical textural features of pre-existing saddle dolomite (e.g. sweeping extinction, curved crystal faces, etc.) can be seen. The chemical composition is ($Ca_{0.972}$ $Mg_{0.023}$ $Fe_{0.005}$ $Mn_0$) $CO_3$ ($n=39$). $\delta^{18}O$ has values from −8.61 to −6.76 (with one more negative value

Table 1
Summary of the petrographic, cathodoluminescence, geochemical, fluid inclusions and isotopic data of different calcite and dolomite phases

| | | Petrography | CL | Chemical composition | Th (°C) | Salinity (wt.% NaCl eq.) | $^{18}O$ (VPDB) | $^{13}C$ (VPDB) | $^{87}Sr/^{86}Sr$[a] |
|---|---|---|---|---|---|---|---|---|---|
| Vertical veins | Calcite matrix and allochems (Host rock) | 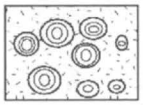 | dark red | $(Ca_{0.982}\ Mg_{0.016}\ Fe_{0.003}\ Mn_0)\ CO_3$ (n=10) | --- | --- | -7.19 to -4.86 | +1.62 to +2.28 | 0.70723 to 0.70736 |
| | Echelon tension gashes calcite cement |  | non luminiscent to dark red | $(Ca_{0.983}\ Mg_{0.010}\ Fe_{0.007}\ Mn_0)\ CO_3$ (n=12) | --- | --- | -11.37 | +1.06 | --- |
| | Rhombic dolomite replacement cement | 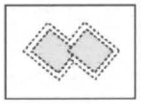 | core: black non luminescent; outer zone: thin bright orange alternating with bright yellow calcite | $(Ca_{0.548}\ Mg_{0.415}\ Fe_{0.036}\ Mn_0)\ CO_3$ (n=11) | --- | --- | --- | --- | --- |
| | Saddle dolomite replacement cement | 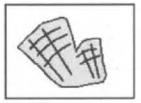 | dull brown to non luminescent | $(Ca_{0.537}\ Mg_{0.448}\ Fe_{0.015}\ Mn_0)\ CO_3$ (n=48) | *primary FI:* 110 to 155; mode=125 | *primary FI:* 21.5 to 23.5; mode=22.5 | -11.54 to -11.28 | +2.13 to +2.22 | 0.70748 to 0.70857 |
| | Dedolomite | 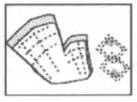 | bright yellow calcite zones and scattered non luminiscent patches | $(Ca_{0.972}\ Mg_{0.023}\ Fe_{0.005}\ Mn_0)\ CO_3$ (n=39) | --- | --- | -12.25 to -6.76 | -4.38 to +0.20 | 0.70806 to 0.70845 |
| | Calcite cement |  | zoned dark-red and red calcite and non luminescent pore filling/replacing calcite | $(Ca_{0.985}\ Mg_{0.012}\ Fe_{0.004}\ Mn_0)\ CO_3$ (n=73) | *primary FI:* 160 to 260; mode=170 | *primary FI:* 5.5 to 9.5; mode=7 | -13.45 to -9.97 | +0.10 to +1.80 | 0.70796 to 0.70801 |
| | Bed-parallel stylolite calcite cement | 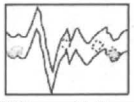 | outer zone: bright yellow calcite; inner zone: dull orange calcite | $(Ca_{0.986}\ Mg_{0.011}\ Fe_{0.003}\ Mn_0)\ CO_3$ (n=46) | --- | --- | -8.81 | +0.79 | 0.70775 |

[a] Tithonian–Berriasian belemnites (Jenkyns et al., 2002): 0.70715 to 0.70725.

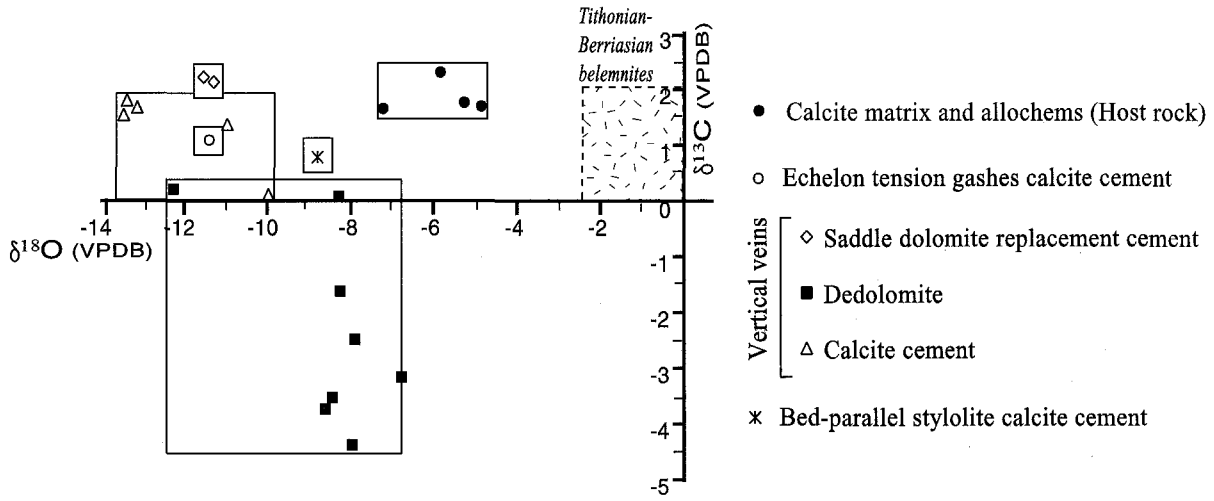


Fig. 2. Oxygen and carbon isotope data for calcite and dolomite phases. The box represents the range for Tithonian–Berriasian belemnites (Jenkyns et al., 2002).

of $-12.25$) and $\delta^{13}C$ from $-4.38$ to $+0.20$. The obtained data (Fig. 2) shows a typical meteoric trend (Heydari, 1997; Al-Aasm, 2000).

*3.2.1.4. Calcite cement.* This cement fills vertical fractures and postdates the rhombic, saddle dolomite and dedolomite phases. This calcite displays textures ranging from small palisade crystals (perpendicular to vein wall) to drusy (50 to 300 μm) and coarse mosaics composed by equant crystals (1.5 to 2.6 mm). The chemical composition is ($Ca_{0.985}$ $Mg_{0.012}$ $Fe_{0.004}$ $Mn_0$) $CO_3$ ($n=73$). Primary fluid inclusions ($H_2O$–NaCl) have one high value of 260 °C and four values that cluster around $160 \pm 10$ °C (mode = 170) with salinities from 5.5 to 9.5 wt.% NaCl eq. (mode = 7). Th values are considerably higher than those measured in saddle dolomite. $\delta^{18}O$ values are the most negative values of all the phases ($-13.45$ to $-9.97$) and this phase shows slightly positive $\delta^{13}C$ ($+0.10$ to $+1.80$).

*3.2.2. Bed-parallel stylolites calcite cement*

This cement fills bed-parallel stylolites that acted as extensional veins developed during the later Alpine compression stress field (ESE trend; Alvaro et al., 1979; Liesa and Simón, 1994) and are associated to the transversal stylolites. Two textural types characterize this calcite. When in contact with the host rock, the crystals are elongated, anhedral and display a bright yellow colour under CL. Occasionally, these crystals are very cloudy with Fe-oxides inclusions that retain the "rhombic texture" and contain relicts of dolomite. However, the central part of the stylolite-veins contains a mosaic of big clean calcite crystals which show curved faces and slightly sweeping extinction with dull orange luminescence. Crystals with curved faces have been observed at the boundary with the host rock. The chemical composition for both types is ($Ca_{0.986}$ $Mg_{0.011}$ $Fe_{0.003}$ $Mn_0$) $CO_3$ ($n=46$). The $\delta^{18}O$ value is $-8.81$ and the $\delta^{13}C$ value is $+0.79$. This value (Fig. 2) must be considered carefully because it may reflect mixture of the two textural types describes above.

## 4. Strontium isotopes

Calcite matrix and allochems (host rock) have $^{87}Sr/^{86}Sr$ ratios that range from 0.70723 to 0.70736 and are slightly higher than the Tithonian–Berriasian belemnites (0.70715 to 0.70725) reported by Jenkyns et al. (2002). Moreover, the calcites and dolomites analysed always have higher values than the host rock and the standard belemnites. The saddle dolomite and dedolomite are enriched in radiogenic Sr (see Table 1).

## 5. Discussion and conclusions

A period of fault-controlled rapid syn-rift subsidence occurred after deposition of the Bovalar Formation (Salas et al., 2001). This stage probably caused the development of the bed-parallel stylolites due to geostatic pressure. However, the presence of calcite-filled echelon tension gashes that are cross-cut by parallel stylolites demonstrates a component of dextral shear associated with vein dilatation suggesting an early predominantly distensional stress regime (Alvaro et al., 1979; Liesa and Simón, 1994). Several stages of dolomitization are described for the Salzedella sub-basin in the Tithonian–Berriasian and Aptian age. The dolomitization has been related to fractures and unconformities and characterized by geochemical data ($\delta^{18}O$, $^{87}Sr/^{86}Sr$ and fluid inclusions). The interpretation is based on a combination of topographic and advection-driven flow system in which meteoric waters descend to the Triassic and Liassic evaporite levels where they mix with connate waters and ascend due to increased heat flows at the end of the Late Jurassic–Early Cretaceous rift stage (Nadal, 2001).

The present paper describes another dolomitization event that occurred in relation to the later Alpine deformation. The vertical veins were filled by multiple phases of replacement cements, including saddle dolomite and calcite cement. These phases can be considered "hydrothermal" in the sense of Machel and Lonnee (2002), based on their Th values (125 and 170 °C, respectively), negative $\delta^{18}O$ values ($-11.54$ to $-11.28$‰ VPDB and $-13.45$ to $-9.97$‰ VPDB) and $^{87}Sr/^{86}Sr$ values that are higher than in the host rock. Our conclusion is also supported by the burial and thermal model proposed by Permanyer et al. (2001) for the Salzedella sub-basin, which has experienced the most subsidence in the Maestrat Basin. These authors reported a maximum temperature of 110 °C (confirmed by vitrinite reflectance and FI data) for the Bovalar Formation.

The general isotopic trend and salinities of fluid inclusions indicate a mix of saline waters, possibly derived from the underlying Triassic and Liassic evaporites, with deep circulating meteoric water that is probably related to the regional Alpine compression.


## Acknowledgements

Funding was provided by research project DGICYT BTE2000-0574-C03-02, Ph.D. Grant (MECyD) to M.A. Caja and by the Natural Sciences and Engineering Research Council of Canada (NSERC) to I. Al-Aasm. Special thanks goes to R.A.J. Swennen and an anonymous referee for the constructive review of the manuscript.


## References


Al-Aasm, I.S., 2000. Chemical and isotopic constraints for recrystallization of sedimentary dolomites from the Western Canada Sedimentary Basin. Aquatic Geochemistry 6, 227–248.

Al-Aasm, I.S., Taylor, B.E., South, B., 1990. Stable isotope analysis of multiple carbonate samples using selective acid extraction. Chemical Geology 80, 119–125.

Alvaro, M., Capote, R., Vegas, R., 1979. Un modelo de evolución geotectónica para la cadena Celtibérica. Acta Geológica Hispánica 14, 172–181.

Heydari, E., 1997. Hydrotectonic models of burial diagénesis in platform carbonates based on formation water geochemistry in North American sedimentary basins. Basin-Wide Diagenetic Patterns: Integrated Petrologic, Geochemical and Hydrologic Considerations. SEPM Special Publication, vol. 57, pp. 53–79.

Jenkyns, H.C., Jones, C.E., Gröcke, R., Hesselbo, S., Parkinson, D.N., 2002. Chemostratigraphy of the Jurassic System: applications, limitations and implications for palaeoceanography. Journal of the Geological Society, London 159, 351–378.

Liesa, C.L., Simón, J.L., 1994. Fracturación a distintas escalas y campos de esfuerzos durante la tectogénesis alpina en el área de Mosqueruela (Teruel). Estudios Geológicos 50 (1–2), 47–57.

Machel, H.G., Lonnee, J., 2002. Hydrothermal dolomite—a product of poor definition and imagination. Sedimentary Geology 152, 163–171.

Nadal, J., 2001. Estudi de la dolomització del Juràssic superior-Cretaci inferior de la cadena ibérica oriental i la cadena costanera catalana: Relació amb la segona etapa de rift mesozoica. Tesi doctoral, Univ. de Barcelona. 443 pp.

Permanyer, A., Salas, R., Rossi, C., 2001. Contribution of organic geochemistry to integrated studies on sedimentary basin evolution. In: Lago, M., Arranz, E., Galé, C. (Eds.), III Congreso Ibérico de Geoquímica, VIII Congreso de Geoquímica de España. Instituto Tecnológicode Aragón, Zaragoza, pp. 113–125.

Salas, R., Guimerà, J., Mas, R., Martín-Closas, C., Meléndez, A., Alonso, A., 2001. Evolution of the Mesozoic Central Iberian Rift System and its Cenozoic inversion (Iberian Chain). In: Ziegler, P.A., Cavazza, W., Robertson, A.H.F., Crasquin-Soleau, S. (Eds.), Peri-Tethys Memoir 6: Peri-Tethyan Rift/Wrench Basins and Passive Margins. Mém. Mus. Natn. Hist. Nat., vol. 186, pp. 145–185.